RSC Advances

PAPER

View Article Online
View Journal | View Issue

Cite this: RSC Adv., 2017, 7, 2019

Synthesis, structure and magnetic properties of $(Eu_{1-x}Mn_x)MnO_{3-\delta}$†

Jianming Deng,[b] Aimei Yang,[b] M. A. Farid,[a] Hao Zhang,[a] Jian Li,[a] Hongxing Zhang,[a] Guobao Li,*[a] Laijun Liu,*[b] Junliang Sun[a] and Jianhua Lin*[a]

Received 28th October 2016
Accepted 6th December 2016

DOI: 10.1039/c6ra25951k

www.rsc.org/advances

The solid solution $(Eu_{1-x}Mn_x)MnO_{3-\delta}$ ($0 \le x \le 0.126$) has been synthesized using a conventional solid-state method. Powder X-ray diffraction and selected area electron diffraction data reveal that all samples crystallize in the space group *Pnma*. Magnetic measurements indicate that the temperature of the paramagnetic to antiferromagnetic phase transition increases with an increase of Mn in the Eu sites. The neutron diffraction data for $^{153}EuMnO_3$ at 3 K confirmed that the magnetic structure of $EuMnO_3$ at low temperature is a canted A-type antiferromagnetic structure with the magnetic space group *Pnma*1′.

Introduction

Studies of $LnMnO_3$ (Ln = Y, Eu, Gd, Tb, Dy, Ho, Er, Tm, Yb, Lu) have been enhanced after the discovery of both magnetic and ferroelectric order (called multiferroics) in $TbMnO_3$,[1] $YMnO_3$,[2] and $HoMnO_3$.[3] Lots of studies have focused on the doping of $LnMnO_3$ (ref. 4–10) at the Ln and/or Mn sites to find better multiferroics. Particularly, several reports indicate that Mn can be doped into the Ln site.[11–17] This may help us to understand that the properties of $LnMnO_3$ reported in the literature can be different because the composition may be different. Therefore, it should be very useful to have a systematic study on the relationship between the properties and the composition of $Ln_{1-x}Mn_xMnO_3$. Although it is known that Mn can be doped into the Eu site of $EuMnO_3$,[18] detailed studies are fewer. In addition, our previous work[15–17] has indicated that $Tb_{1-x}Mn_yMnO_3$ can show very interesting magnetic properties. Therefore, careful studies into the synthesis, structure and magnetic properties of Mn doped $EuMnO_3$ are performed. The details are presented below.

Experimental

Samples with the nominal formula $(Eu_{1-x}Mn_x)MnO_{3-\delta}$ ($x = 0$, 0.025, 0.05, 0.075, 0.1, 0.125 and 0.15) (named M1, M2, M3, M4, M5, M6 and M7, respectively) were synthesized using a traditional solid-state reaction from stoichiometric amounts of Eu_2O_3 (99.95%) or $^{153}Eu_2O_3$ (99.995%), and $MnCO_3$ (A.R.). Here the formula is noted as $(Eu_{1-x}Mn_x)MnO_{3-\delta}$ instead of $(Eu_{1-x}Mn_x)MnO_3$ to highlight that the oxygen component is not exactly analyzed. Some oxygen vacancies may appear in the samples. The oven-dried reagents were mixed and homogenized through about thirty minutes of grinding with an agate mortar and a pestle. The mixtures were subjected to 6 h of calcination at 800 °C. They were then pressed into pellets to undergo four 12 h heat treatments at 1200 °C, followed by a furnace cooling every time with intermediate grinding. All the treatments were carried out under air. The weights of the samples were monitored before and after heat treatment. The maximum difference was about 4 mg for the 6 g samples. Therefore, the final compositions of the samples were considered the same as the initial ones. Powder X-ray diffraction (PXRD) data were collected on a PANalytical X'Pert[3] Powder diffractometer with Cu $K\alpha_\alpha$ ($\lambda_1 = 0.15405$ nm and $\lambda_2 = 0.15443$ nm) radiation (2θ range: 5–120° for 2 h; step size: 0.0131°) at 40 kV and 40 mA at room temperature. Neutron powder diffraction (NPD) data for $^{153}EuMnO_3$ were collected on the instrument Echidna at the OPAL reactor (Lucas Heights, Australia) at the Australian Nuclear Science and Technology Organization (ANSTO), at $\lambda = 1.62150$ Å. The X-ray diffraction data were analyzed using GSAS software.[19,20] The magnetic properties were investigated using a Cryogenic physical property measurement system (PPMS) from 2 to 300 K. Selected area electron diffractions (SAED) were carried out on a JEM2100F, with a 200 kV accelerating voltage. The X-ray photoelectron spectroscopy (XPS) patterns were obtained with a UK Kratos AxisUltra spectrometer with an Al Kα X-ray source operating at 15 kV and 15 mA. The chamber pressure was less than 5.0×10^{-9} torr. Electron binding energies were calibrated against C 1s emission at $E_b = 284.8$ eV.

[a]Beijing National Laboratory for Molecular Sciences, State Key Laboratory of Rare Earth Materials Chemistry and Applications, College of Chemistry and Molecular Engineering, Peking University, Beijing 100871, P. R. China. E-mail: liguobao@pku.edu.cn

[b]College of Materials Science and Engineering, Guilin University of Technology, Guilin 541004, China

† Electronic supplementary information (ESI) available. See DOI: 10.1039/c6ra25951k

Results and discussion

Solid solution of $(Eu_{1-x}Mn_x)MnO_{3-\delta}$

The X-ray diffraction patterns of the studied samples are shown in Fig. 1. The data for M1 to M6 are very similar, with the reflections moving systematically to a higher angle when more Mn is in the samples. These patterns agree well with that reported for $EuMnO_3$ (ref. 21) in the space group *Pnma*, which indicates that the space group *Pnma* may be fitted to describe the structure of these samples. After considering that the true structure for a Perovskite compound is very complex,[22–24] selected area electron diffraction (SAED) patterns of the above samples have been obtained and analyzed. The typical data are shown in Fig. 2, which confirm that the space group *Pnma* can be used to describe the structure of M1 to M6. Then the structure of $EuMnO_3$ is used to refine the corresponding data, with the supposition that some Mn occupies Eu sites, using the Rietveld method using GSAS. Good refinement is obtained for all of the data with $R_{wp} \leq 0.023$ and $R_p \leq 0.013$ (the corresponding data is listed in Tables S1 and S2 in the ESI†). Typical Rietveld plots are shown in Fig. 3. For M7, a small amount of Mn_3O_4 impurity was detected, which has been marked in Fig. 3d. Then a two phase model is used to refine the data for M7.

As shown in Fig. 4, with an increase in Mn in $(Eu_{1-x}Mn_x)MnO_{3-\delta}$, the lattice parameters a and c decrease, and b increases, which agrees well with Vegard's law:[25,26]

$$a_{Ox} = a_{O0}(1 - x) + a_{O1}x \quad (1)$$

$$b_{Ox} = b_{O0}(1 - x) + b_{O1}x \quad (2)$$

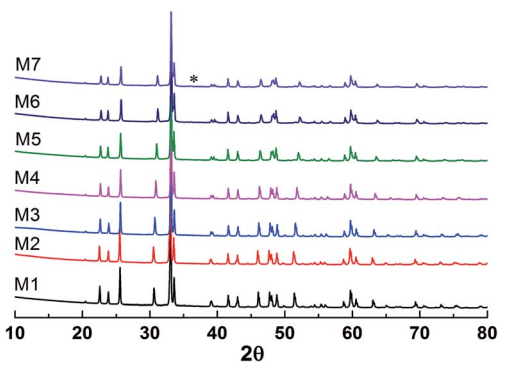

Fig. 1 Powder X-ray diffraction patterns of the samples with the nominal formula $(Eu_{1-x}Mn_x)MnO_{3-\delta}$. * reflections from the impurity.

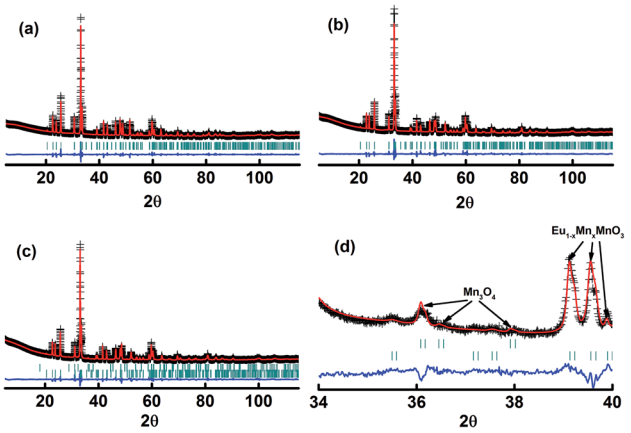

Fig. 3 Rietveld plots of the powder X-ray diffraction patterns for the samples M1 (a), M6 (b), and M7 (c and d). The symbol "+" represents the observed value, the solid line represents the calculated value, the marks below the diffraction patterns are the calculated reflection positions, and the difference curve is shown at the bottom of the figure.

$$c_{Ox} = c_{O0}(1 - x) + c_{O1}x \quad (3)$$

where $a_{Ox}(b_{Ox}, c_{Ox})$, $a_{O0}(b_{O0}, c_{O0})$, and $a_{O1}(b_{O1}, c_{O1})$ are the lattice parameters a (b, c) of orthorhombic $(Eu_{1-x}Mn_x)MnO_{3-\delta}$, pure orthorhombic $EuMnO_3$ and supposed orthorhombic $MnMnO_3$. x is the composition variable, given by Mn/(Eu + Mn). Using the data shown in Fig. 4 and eqn (1)–(3), the maximum value for x in the solid solution $(Eu_{1-x}Mn_x)MnO_{3-\delta}$ is found to be 0.126. That is, the range for the solid solution $(Eu_{1-x}Mn_x)MnO_{3-\delta}$ is $0 \leq x \leq 0.126$. The lattice parameters of the solid solution $(Eu_{1-x}Mn_x)MnO_{3-\delta}$ follow well the relationship $b/\sqrt{2} < c < a$, which indicates that the solid solution $(Eu_{1-x}Mn_x)MnO_{3-\delta}$ belongs to an orthorhombic OI structure.[27]

XPS data for $(Eu_{1-x}Mn_x)MnO_{3-\delta}$

In order to assess the oxidation states of Eu and Mn in the samples, XPS analysis has been performed. The corresponding data are shown in Fig. 5. The XPS spectra for Eu 3d in the samples M1 to M6 are almost the same. The two peaks at around 1135.6 and 1165.2 eV are attributed to Eu $3d_{5/2}$ and Eu $3d_{3/2}$, which indicates that the valence state of Eu in the samples is +3.[28,29] The XPS spectra of Mn 2p are also almost the same for all six samples, as shown in Fig. 5b. The corresponding Mn $2p_{3/2}$ peak is located at about 641.9 eV, which agrees well with the

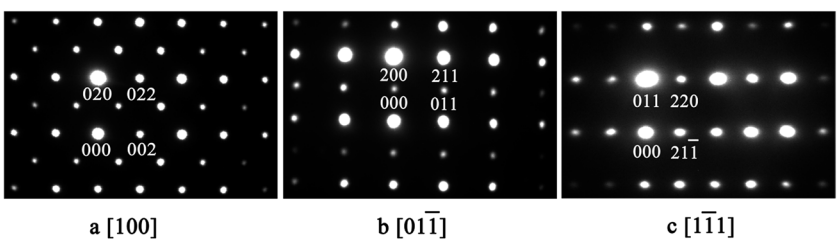

Fig. 2 Selected area electron diffraction patterns of M5 along the [100], [$01\bar{1}$], and [$1\bar{1}1$] directions in the space group *Pnma*.

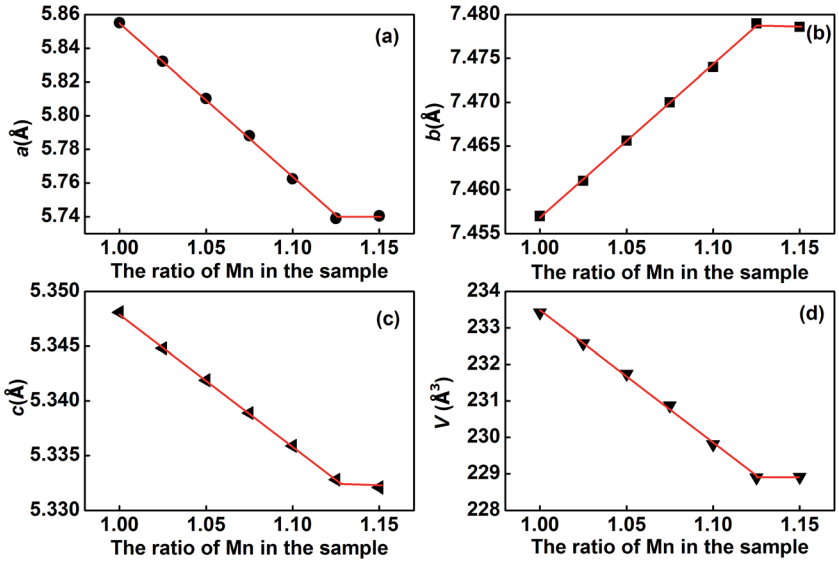

Fig. 4 Variation of the lattice parameters *a* (a), *b* (b), *c* (c) and the volume of the unit cell *V* (d) for the solid solution $(Eu_{1-x}Mn_x)MnO_{3-\delta}$.

binding energy of Mn $2p_{3/2}$ in α-Mn_2O_3.[30,31] Thus, the valence state of Mn is +3 in the solid solution $(Eu_{1-x}Mn_x)MnO_{3-\delta}$.

Magnetic properties

As reported previously,[32] "negative magnetization" in the ZFC (zero field cooling) curve can be easily observed for M1 ($EuMnO_3$), which is attributed to the effect of a trapped negative field in the solenoid of a superconducting magnet. Two characteristic temperatures can be assigned to M1: the temperature where the ZFC and FC (field cooling) curves start to depart, which is attributed by us to the phase transition temperature from PM to AFM, noted as T_{N1}, which is 52 K; and the peak temperature in the ZFC curves, which is attributed to the phase transition temperature from AFM to cAFM, noted as T_{N2}, which is 45 K, as listed in Table 1. These values agree well with data reported by other researchers.[33–36]

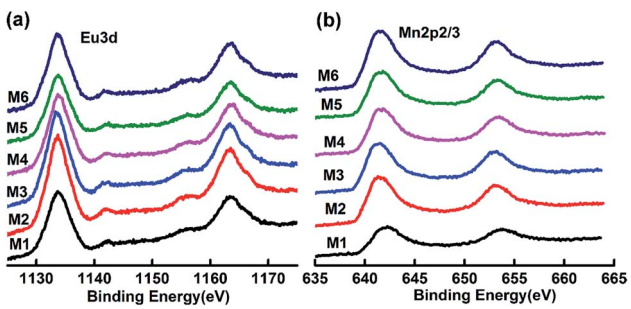

Fig. 5 XPS spectra of Eu $3d_{5/2}$ (a) and Mn $2p_{3/2}$ (b) for M1 to M6.

Table 1 The T_{N1}, T_{N2}, Curie constant (*C*), θ, μ_{cal}, and μ_{exp} for M1 to M6

Sample	M1	M2	M3	M4	M5	M6
T_{N1} (K)	52	53	55	58	64	70
T_{N2} (K)	45	42	32	40	42	42
C (emu mol^{-1} K)	4.87	5.10	5.18	5.21	5.24	5.25
θ (K)	−84	−54.0	−48.6	−36.1	−19.6	−21.9
μ_{cal} (μ_B)	5.96	5.99	6.02	6.04	6.07	6.09
μ_{exp} (μ_B)	6.24	6.39	6.44	6.45	6.47	6.48

With an increase of Mn in the samples, the "negative magnetization" in the ZFC curve disappears, as shown in Fig. 6. Similarly to M1 ($EuMnO_3$), two characteristic temperatures, T_{N1} and T_{N2}, can be obtained from the temperature dependence of the magnetic susceptibility in the samples M2 to M6 in ZFC and FC modes, which are listed in Table 1. It is found that with an increase of Mn in the system, the PM to AFM phase transition temperature, T_{N1}, increases. This means that Mn is a good dopant to increase T_{N1} in $Eu_{1-x}Mn_xMnO_{3-\delta}$. A similar phenomenon is also found for Mn doped $TbMnO_3$.[17]

The linearity of $\chi^{-1}(T)$ above the temperature T_{N1} shown in Fig. 6d–f suggests that the reciprocal magnetic susceptibility follows the Curie–Weiss (CW) law, $\chi = C/(T-\theta)$, where χ is the magnetic susceptibility of the paramagnetic phase, C is the Curie constant, T is the temperature, and θ is the Weiss constant. The corresponding Curie constants C, Weiss constants θ and effective paramagnetic moments are obtained and presented in Table 1. The effective magnetic moment calculated from the Curie constant C increases with an increase in Mn in the sample, and agrees well with the expected value under the supposition[37] that $\mu_{eff}{}^2 = (1+x)\mu_{eff}{}^2(Mn^{3+}) + (1-x)\mu_{eff}{}^2(Eu^{3+})$, with $\mu(Mn^{3+}) = 4.90\ \mu_B$, and $\mu(Eu^{3+}) = 3.40\ \mu_B$. The obtained Weiss constant θ is negative, which indicates that the magnetic interaction is antiferromagnetic in nature.

The magnetic hysteresis loops at selected temperatures have been measured and typical data are shown in Fig. 7. The magnetic hysteresis loops show a clear butterfly shape at 10 K, indicating that the samples are metamagnetic at this temperature. The maximum magnetization value, at $H = 7$ T at 10 K, increases from 12.8 to 38.9 emu g^{-1} with an increase in Mn content from 0.025 to 0.125, indicating that doping of Mn at the Eu site makes $Eu_{1-x}Mn_xMnO_3$ easier to magnetize, which is similar to $Eu_{1-x}Y_xMnO_3$ (ref. 4) and $Eu_{1-x}Sr_xMnO_3$.[38]

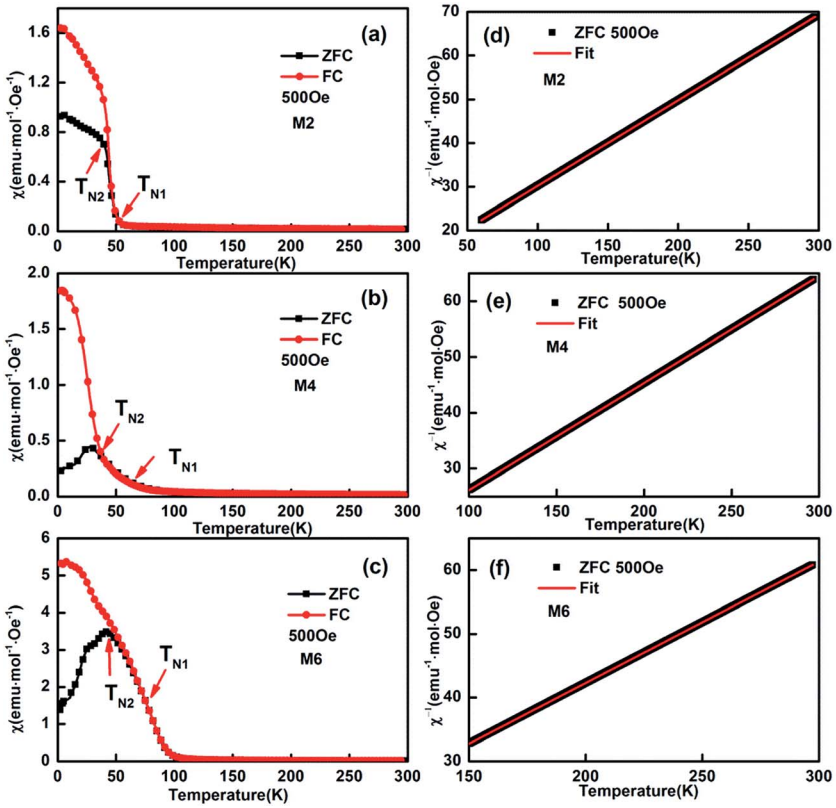

Fig. 6 Typical temperature dependence of the magnetization of $(Eu_{1-x}Mn_x)MnO_{3-\delta}$: $\chi-T$ and $\chi^{-1}-T$ curves for M2 (a and d), M4 (b and e), and M6 (c and f), respectively.

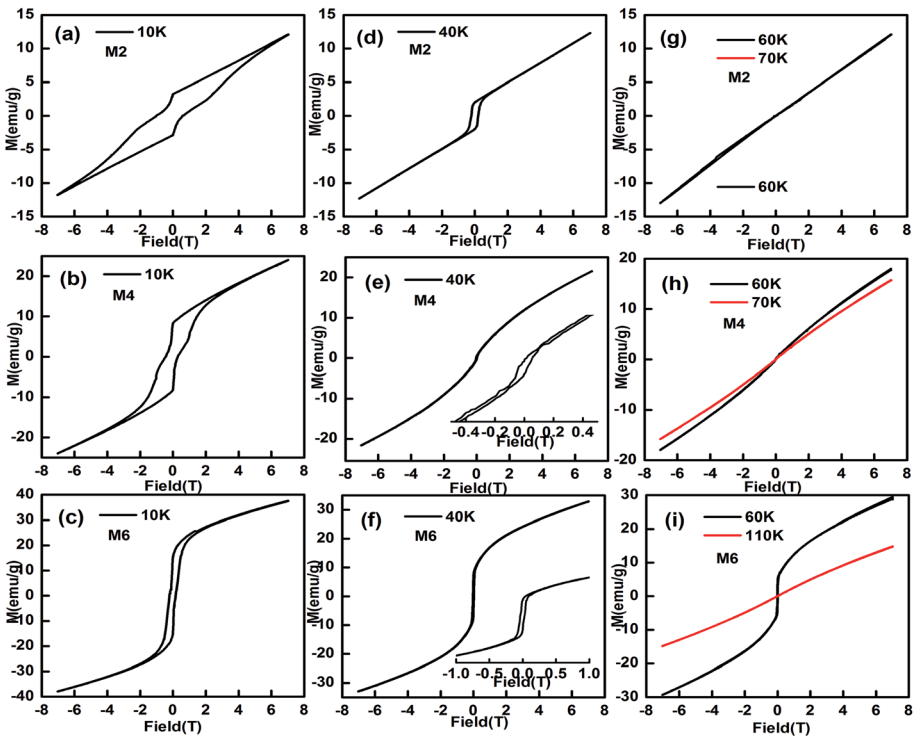

Fig. 7 The magnetic hysteresis loops for M2, M4 and M6 ($(Eu_{1-x}Mn_x)MnO_{3-\delta}$, $x = 0.025$ (a, d, g), 0.075 (b, e, h), and 0.125 (c, f, i)) at selected temperatures.

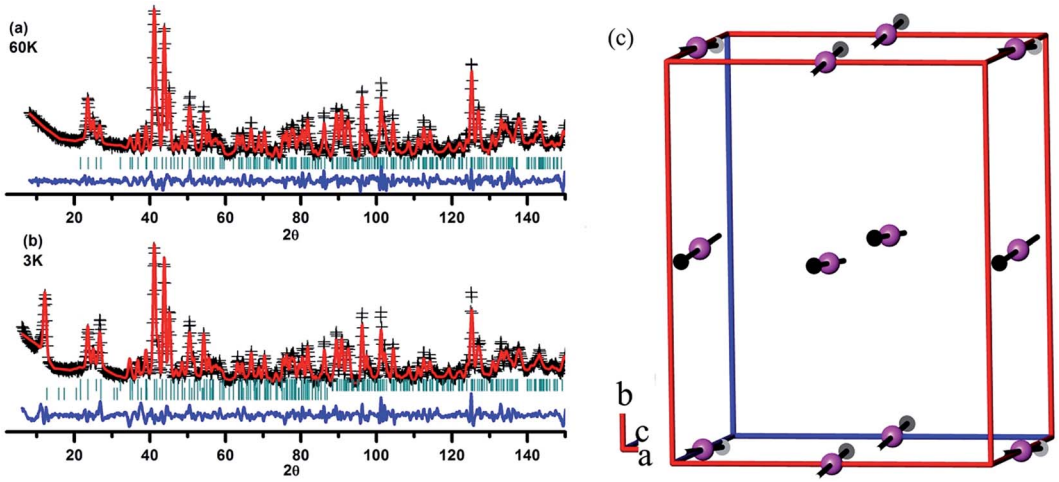

Fig. 8 Rietveld plots of the neutron diffraction data from $^{153}EuMnO_3$ at 60 K (a) and 3 K (b), and the magnetic structure of $^{153}EuMnO_3$ at 3 K (c).

When the temperature increases, the butterfly shape of the *M–H* curve changes to a normal shape, as shown in Fig. 7d–f, which indicates that the samples become canted antiferromagnetic, rather than metamagnetic. At 60 K, a straight line is observed for M2 and M3, which agrees well with the finding that the PM to AFM phase transition temperature T_{N1} for M2 and M3 is lower than 60 K, as listed in Table 1. But for M4, M5, and M6, the *M–H* curves are not straight lines at 60 K.

Neutron diffraction of $^{153}EuMnO_3$

As mentioned previously,[32,39] it is hard to get neutron diffraction data for $EuMnO_3$ because the neutrons can be absorbed by Eu. Therefore, the magnetic structure of $EuMnO_3$ has not been solved until now, although T. Goto *et al.*[34] have predicted that it has a phase transition from PM to ICAFM (incommensurate antiferromagnetic) at ~50 K, and a further transition from ICAFM to cAAFM (canted A-type antiferromagnetic) ordering at ~44 K. It has been reported that neutron diffraction data can be obtained for $^{153}EuMnO_3$,[39] where only data from around room temperature has been presented, which confirms that $^{153}EuMnO_3$ crystallizes in the space group *Pnma*. Therefore, $^{153}EuMnO_3$ has been synthesized in our lab and sent away for neutron diffraction data collection at 60 and 3 K. As shown in Fig. 8a, the neutron diffraction data for $^{153}EuMnO_3$ at 60 K can be refined well using the space group *Pnma* with the parameters listed in Table 2, which may indicate that the structure of $^{153}EuMnO_3$ does not change between 300 K and 60 K. However, new diffraction peaks are found in the neutron data from $^{153}EuMnO_3$ at 3 K, which can be attributed to the A-type[40] magnetic ordering of Mn in $^{153}EuMnO_3$, as shown in Fig. 8c with the refinement parameters listed in Table 2. In the first work on the magnetic structure of Mn in the doped perovskite $LaMnO_3$, E. O. Wollan *et al.*[40] established a note system of A, B, C, D, E, F, and G type to note the different possible magnetic structures of Mn. Specially, A-type magnetic ordering means that the magnetic moment arrangement of Mn is similar to that shown in Fig. 8c. That is, the magnetic moments of the four-close-neighboring Mn in the first and the second layer are inversed. As shown in Fig. 8c, the moment of Mn in the first layer directs to the positive *c*-axis, while the moment of Mn in the

Table 2 Rietveld refinement details for the neutron diffraction data from $^{153}EuMnO_3$ at 60 K and 3 K

	60 K	3 K
Phase 1	Nuclear phase	Nuclear phase
Space group	*Pnma*	*Pnma*
Lattice parameters (Å)	$a = 5.8217(2)$, $b = 7.2138(3)$, $c = 5.3242(8)$	$a = 5.8183(2)$, $b = 7.2082(3)$, $c = 5.3269(2)$
Atom	*x*, *y*, *z*	*x*, *y*, *z*
Eu	0.0787(3), 0.2500, 0.9844(3)	0.0800(3), 0.2500, 0.9845(3)
Mn	0.0000, 0.0000, 0.5000	0.0000, 0.0000, 0.5000
O1	0.4722(3), 0.2500, 0.0957(3)	0.4678(3), 0.2500, 0.0974(3)
O2	0.3236(3), 0.0462(3), 0.7063(3)	0.3249(3), 0.0478(3), 0.7066(3)
Phase 2		Magnetic phase
Space group		*Pnma*1′
Lattice parameters (Å)		$a = 5.8183(2)$, $b = 7.2082(3)$, $c = 5.3269(2)$
Atom		$(x, y, z)/(M_x, M_y, M_z)$
Mn		(0.0000, 0.0000, 0.5000)/(−0.554, 0.190, 2.868)
R factor[a]	$R_{wp} = 0.033$, $R_p = 0.026$	$R_{wp} = 0.041$, $R_p = 0.031$

[a] R_p is sum($|I_0 - I_C|$)/sum(I_0), and R_{wp} is the weighted *R* factor for the neutron diffraction data.

second layer directs to the negative *c*-axis. Our results confirm the prediction of a cAAFM phase for $EuMnO_3$ by T. Goto *et al.*[34] More careful studies are planned to confirm the ICAFM phase for $^{153}EuMnO_3$.

Conclusions

Solid solution $Eu_{1-x}Mn_xMnO_{3-\delta}$ has been synthesized using a conventional solid state method at 1200 °C under air. The powder X-ray diffraction and selected area electron diffraction data confirm that all samples crystallize in the space group *Pnma* at room temperature. The range of x for the solid solution obtained in the present case is assessed to be $0 \leq x \leq 0.126$. With the doping of Mn in the Eu site, the paramagnetic to antiferromagnetic phase transition moves to a higher temperature. In addition, the neutron diffraction data from $^{153}EuMnO_3$ at 3 K confirmed that the magnetic structure of $EuMnO_3$ at low temperatures is canted A-type antiferromagnetic.

Acknowledgements

This work is supported by the National Key Basic Research Project of China (2010CB833103), and the National Natural Science Foundation of China (Grants 21271014, 11275012). We thank Dr M. Avdeev for assistance in collecting the neutron power diffraction data at the OPAL facility.

References

1 T. Kimura, T. Goto, H. Shintani, K. Ishizaka, T. Arima and Y. Tokura, *Nature*, 2003, **426**, 55.
2 M. Fiebig, T. Lottermoser, D. Fröhlich, A. V. Goltsev and R. V. Pisarev, *Nature*, 2002, **419**, 818.
3 T. Lottermoser, T. Lonkai, U. Amann, D. Hohlwein, J. Ihringer and M. Fiebig, *Nature*, 2004, **430**, 541.
4 J. Hemberger, F. Schrettle, A. Pimenov, P. Lunkenheimer, V. Y. Ivanov, A. A. Mukhin, A. M. Balbashov and A. Loidl, *Phys. Rev. B: Condens. Matter Mater. Phys.*, 2007, **75**, 035118.
5 V. Cuartero, J. Blasco, J. García, G. Subías, C. Ritter and J. Alberto Rodríguez-Velamazán, *Phys. Rev. B: Condens. Matter Mater. Phys.*, 2010, **81**, 224117.
6 D. O'Flynn, C. V. Tomy, M. R. Lees, A. Daoud-Aladine and G. Balakrishnan, *Phys. Rev. B: Condens. Matter Mater. Phys.*, 2011, **83**, 174426.
7 H. D. Zhou, J. C. Denyszyn and J. B. Goodenough, *Phys. Rev. B: Condens. Matter Mater. Phys.*, 2005, **72**, 224401.
8 P. P. Rout, S. K. Pradhan and B. K. Roul, *Ceram. Int.*, 2014, **40**, 9647.
9 A. Nandy and S. K. Pradhan, *Dalton Trans.*, 2015, **44**, 17229.
10 A. Astudillo, J. Izquierdo, F. J. Bonilla, G. Bolaños and O. Morán, *IEEE Trans. Magn.*, 2013, **49**, 4590.
11 E. Pollert and Z. Jirak, *J. Solid State Chem.*, 1980, **35**, 262.
12 G. Lescano, F. M. Figueiredo, F. M. B. Marques and J. Schmidt, *J. Eur. Ceram. Soc.*, 2001, **21**, 2037.
13 I. Gélard, N. Jehanathan, H. Roussel, S. Gariglio, O. I. Lebedev, G. Van Tendeloo and C. Dubourdieu, *Chem. Mater.*, 2011, **23**, 1232.
14 A. N. Ulyanov, N. E. Pismenova, D. S. Yang, V. N. Krivoruchko and G. G. Levchenko, *J. Alloys Compd.*, 2013, **550**, 124.
15 R. Wang, C. X. Yang, M. Fan, M. M. Wu, C. H. Wang, X. H. Yu, J. L. Zhu, J. R. Zhang, G. B. Li, Q. Z. Huang, D. F. Chen, T. N. Jin, T. Kamiyama, F. H. Liao and J. H. Lin, *J. Alloys Compd.*, 2013, **554**, 385.
16 H. Zhang, R. Flacau, J. L. Sun, G. B. Li, F. H. Liao and J. H. Lin, *Inorg. Chem.*, 2014, **53**, 4535.
17 H. Zhang, R. Flacau, X. Du, P. Manuel, J. Z. Cong, Y. Sun, J. L. Sun, S. H. Yang, G. B. Li, F. H. Liao and J. H. Lin, *ChemPhysChem*, 2016, **17**, 1098.
18 O. M. Fedorova, V. F. Balakirev and Yu. V. Golikov, *Inorg. Mater.*, 2007, **43**, 994.
19 H. M. Rietveld, *J. Appl. Crystallogr.*, 1969, **2**, 65.
20 B. H. Toby, *J. Appl. Crystallogr.*, 2001, **34**, 210.
21 N. V. Kasper and I. O. Troyanchuk, *J. Phys. Chem. Solids*, 1996, **57**, 1601.
22 G. B. Li, S. X. Liu, F. H. Liao, S. J. Tian, X. P. Jing, J. H. Lin, Y. Uesu, K. Kohn, K. Saitoh, M. Terauchi, N. L. Di and Z. H. Cheng, *J. Solid State Chem.*, 2004, **177**, 1695.
23 H. Wang, C. H. Wang, G. B. Li, T. N. Jin, F. H. Liao and J. H. Lin, *Inorg. Chem.*, 2010, **49**, 5262.
24 H. Wang, C. X. Yang, J. Lu, M. M. Wu, J. Su, K. Li, J. R. Zhang, G. B. Li, T. N. Jin, T. Kamiyama, F. H. Liao, J. H. Lin and Y. C. Wu, *Inorg. Chem.*, 2013, **52**, 2388.
25 L. Vegard, *Z. Phys.*, 1921, **5**, 17.
26 L. Vegard, *Z. Kristallogr.*, 1928, **67**, 239.
27 T. S. Chan, R. S. Liu, C. C. Yang, W. H. Li, Y. H. Lien, C. Y. Huang and J. F. Lee, *J. Phys. Chem. B*, 2007, **111**, 2262.
28 Y. U. wamino, T. Ishizuka and H. Yamatera, *J. Electron Spectrosc. Relat. Phenom.*, 1984, **34**, 67.
29 D. F. Mullica, C. K. C. Lok, H. O. Perkins, G. A. Benesh and V. Young, *J. Electron Spectrosc. Relat. Phenom.*, 1995, **71**, 1.
30 M. Oku, K. Hirokawa and S. Ikeda, *J. Electron Spectrosc. Relat. Phenom.*, 1975, **7**, 465.
31 V. Di Castro and G. Polzonetti, *J. Electron Spectrosc. Relat. Phenom.*, 1989, **48**, 117.
32 A. M. Yang, Y. H. Sheng, M. A. Farid, H. Zhang, X. H. Lin, G. B. Li, L. J. Liu, F. H. Liao and J. H. Lin, *RSC Adv.*, 2016, **6**, 13928.
33 I. O. Troyanchuk, N. V. Samsonenko, N. V. Kasper, H. Szymczak and A. Nabialek, *Phys. Status Solidi A*, 1997, **160**, 195.
34 T. Goto, T. Kimura, G. Lawes, A. P. Ramirez and Y. Tokura, *Phys. Rev. Lett.*, 2004, **92**, 257201.
35 W. S. Ferreira, J. A. Moreira, A. Almeida, M. R. Chaves, J. P. Araújo, J. B. Oliveira, J. M. M. Da Silva, M. A. Sá, T. M. Mendonça, P. S. Carvalho, J. Kreisel, J. L. Ribeiro, L. G. Vieira, P. B. Tavares and S. Mendonça, *Phys. Rev. B: Condens. Matter Mater. Phys.*, 2009, **79**, 054303.
36 R. Das and P. Poddar, *RSC Adv.*, 2014, **4**, 10614.
37 J. H. Van Vleck, *J. Appl. Phys.*, 1968, **39**, 365.
38 Y. Tadokoro, Y. J. Shan, T. Nakamura and S. Nakamura, *Solid State Ionics*, 1998, **108**, 261.
39 B. Dabrowski, S. Kolensnik, A. Baszcuk, O. Chmaissem, T. Maxwell and J. Mais, *J. Solid State Chem.*, 2005, **178**, 629.
40 E. O. Wollan and W. C. Koehler, *Phys. Rev.*, 1955, **100**, 545.

